Organic Electronics 13 (2012) 2083–2093

Contents lists available at SciVerse ScienceDirect

Organic Electronics

journal homepage: www.elsevier.com/locate/orgel

Perylene diimides functionalized with N-thiadiazole substituents: Synthesis and electronic properties in OFET devices

Roberto Centore [a,*], Laura Ricciotti [a], Antonio Carella [a], Antonio Roviello [a], Mauro Causà [a], Mario Barra [b], Francesca Ciccullo [b], Antonio Cassinese [b,*]

[a] Department of Chemistry, University of Naples "Federico II", Via Cinthia, I-80126 Naples, Italy
[b] CNR-SPIN and Department of Physics Science, University of Naples "Federico II", Piazzale Tecchio 80, 80125 Naples, Italy

ARTICLE INFO

Article history:
Received 11 February 2012
Received in revised form 5 June 2012
Accepted 5 June 2012
Available online 27 June 2012

Keywords:
Perylene
Thiadiazole
OTFT
FET
Spin coating

ABSTRACT

Two new perylene diimide derivatives N,N′-bis(5-tridecyl-1,3,4-thiadiazol-2-yl)perylene-3,4,9,10-tetracarboxylic 3,4:9,10-diimide (PDI-T1) and N,N′-bis[5-(1-hexyl)nonyl-1,3,4-thiadiazol-2-yl]perylene-3,4,9,10-tetracarboxylic 3,4:9,10-diimide (PDI-T2), achieved by functionalizing the basic perylene molecular core at imide nitrogen with 1,3,4-thiadiazole rings, have been synthesized. Both these compounds make possible the fabrication of n-type organic thin-film transistors able to work in air, even when bare SiO_2 surfaces are utilized as gate dielectric. As active channels of transistors in the bottom-contact bottom-gate configuration, PDI-T1 evaporated films exhibited a maximum mobility of 0.016 cm^2/V s in vacuum. For evaporated PDI-T2 films, instead, mobility values were found to be more than one order of magnitude lower, because of their reduced degree of crystalline order. However, PDI-T2 films can be also deposited by solution techniques and field-effect transistors were fabricated by spin-coating, displaying mobility values ranging between 10^{-6} and 10^{-5} cm^2/V s. Similar to what previously found for other perylene diimide derivatives, our experimental work also demonstrates that the electrical response of both PDI-T1 and PDI-T2 transistors under ambient conditions can be improved by increasing the level of hydrophobicity of the dielectric surface.

1. Introduction

Perylene-3,4,9,10-tetracarboxylic acid diimide (PDI) derivatives represent a class of organic compounds that have been extensively investigated and have found, since the beginning of the last century, wide application in the field of high performance industrial pigments because of their high colour strength, weather fastness and heat stability [1,2]. Today, perylene pigments are mainly used in the coloration of automotive paints, synthetic fibres and engineering resins [3].

PDI derivatives present, as well, a series of other appealing features, such as very high fluorescence quantum efficiency, a strong electron acceptor character, excellent photochemical stability and two photon absorption properties, that make them interesting candidates for use in different fields of organic electronics and photonics: PDI derivatives have so far been used as active materials in newly developed devices as organic thin-film transistors (OTFT) [4–8], fluorescent light collectors [9], organic solar cells [10–12] and optical power limiters [13].

PDI derivatives are characterized by a very energetically stable LUMO frontier orbital and this feature makes them one of the most important class of materials for n-channel OTFT: electron transport in organic thin-film transistors occurs, in fact, through the hopping mechanism between localized LUMO states and the more stable are the latter, the more resistant are the anionic radical charge carriers against electronic traps or oxidation by moisture and oxygen. A value of the LUMO energy between −4.0 and −4.3 eV has been identified as the energetic threshold

* Corresponding authors.
E-mail address: roberto.centore@unina.it (R. Centore).

1566-1199/$ - see front matter © 2012 Elsevier B.V. All rights reserved.
http://dx.doi.org/10.1016/j.orgel.2012.06.002

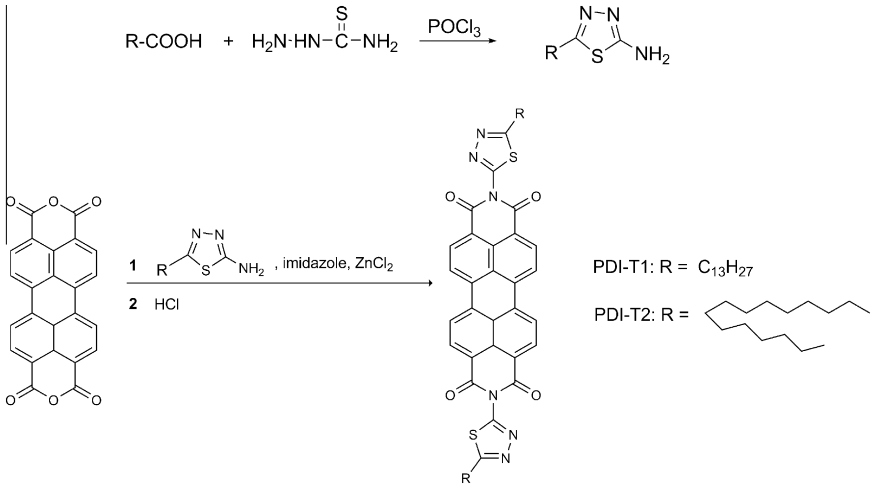

Scheme 1. Molecular structure and synthetic path of the synthesized chromophores.

featured by an organic material to be used as active layer in OTFT efficiently working under ambient conditions [14].

Derivatives of PDI are generally prepared in two different ways, by functionalizing the imide nitrogen or the perylene core (bay substitution) [15]. In both cases, the introduction of strong electron-withdrawing groups has been used to stabilize the LUMO energy of the molecule, but to a different extent. The effect of substitution at imide nitrogen is basically inductive [16], while substitution in the bay position leads to a more dramatic change in both the electronic and optical features of the molecule. At the same time, anyway, even moderate bay substitution produces significant deformation of the planar geometry [17], which can induce negative effects on charge transport [18].

Both the kinds of derivatives have been used for the fabrication of ambient stable OTFT: functionalization of the imide nitrogen with fluoroalkyl [7] or fluorophenyl moieties [8], as well as substitution in the bay position with cyano [5,6] and halogen groups [19], have opened the way to the realization of devices with excellent electrical performance and air stability.

We report here on new PDI derivatives functionalized at the imide nitrogen with a thiadiazole group; their chemical diagrams are shown in Scheme 1, together with the synthetic procedure.

The thiadiazole rings are functionalized with two different alkyl tails, one linear and the other swallow-tail-like in order to increase solubility. The synthesized molecules have been fully characterized for their spectroscopic properties in solution. Then, they were deposited both by evaporation and spin-coating techniques on suitable substrates for the fabrication of n-channel OTFT. The electrical response of these transistors was accurately assessed both in vacuum and under ambient conditions.

2. Experimental

2.1. Materials

All reagents were purchased from Sigma–Aldrich and used without further purification.

2.2. Physico-chemical characterization

Melting and decomposition temperatures were determined respectively by differential scanning calorimetric (DSC) and thermogravimetric (TG) analyses, which were performed using Perkin-Elmer Pyris and TA SDT2960 instruments, under flowing nitrogen, at 10 K/min scanning rate. Temperature controlled optical microscopy was performed with a Zeiss Axioscop polarizing microscope equipped with a Mettler FP90 heating stage. ^{1}H NMR spectra were recorded with a varian spectrometer operating at 200 MHz. Proton chemical shifts were referenced to the residual solvent signal ([D6] DMSO 2.50 ppm). UV/Vis absorption and fluorescence spectra were recorded in chloroform solution respectively with a Jasco V560 spectrophotometer and a Jasco spectrofluorimeter FP750. The fluorescence quantum yield (Φ_f) was determined using quinine sulfate as the standard according to Ref. [20]. Cyclic voltammetry (CV) measurements on thin film were performed using acetonitrile–$NaClO_4$ as the electrolytic solution; redox data were standardized with the Ag/AgCl couple.

Contact angle measurements were performed using a dataphysics OCA 20 system.

2.3. Synthesis

2.3.1. 2-Amino-5-tridecyl-1,3,4-thiadiazole (*1*)

Tetradecanoic acid (62.4 mmol) and thiosemicarbazide (77.9 mmol) were dissolved in $POCl_3$ (21 mL) and stirred at 100 °C for 1 h. The reaction mixture was cooled, diluted with water (94 mL) and refluxed for 4 h. The reaction system was basified using an aqueous solution of sodium hydroxide (1 M) to pH 8 at room temperature. The precipitate was collected by filtration and recrystallized from ethanol–water to afford the final pure product.

Yield: 50% mp: 167–172 °C. ^{1}H NMR (200 MHz, $CDCl_3$): (δ ppm): 0.86 (m, 3H), 1.23 (m, 20H), 1.68, (m, 2H), 2.85 (m, 2H), 6.25 (s, 2H).

2.3.2. 2-Amino-5-(1-hexylnonyl)-1,3,4-thiadiazole (*2*)

2-Hexyldecanoic acid (16.78 g, 65.4 mmol) and thiosemicarbazide (7.446 g, 81.7 mmol) were dissolved in

$POCl_3$ (22 mL) and stirred at 100 °C for 1 h. The reaction mixture was cooled, diluted with water (100 mL) and refluxed for 4 h. The reaction system was basified using an aqueous solution of sodium hydroxide (1 M) to pH 8 at room temperature. The oily phase was extracted with $CHCl_3$ (200 mL), washed again with water (2 × 200 mL) and dried over Na_2SO_4. Finally, the organic solvent was removed at reduced pressure affording pale yellow oil that was used in the next reaction step without further purification.

Yield: 64% ^{1}H NMR (200 MHz, $CDCl_3$): (δ ppm) 0.84 (m, 6H), 1.22 (m, 20H), 1.59, (m, 4H), 2.95 (m, 1H), 5.53 (s, 2H, broad).

2.3.3. N,N′-Bis(5-tridecyl-1,3,4-thiadiazol-2-yl)perylene-3,4,9,10-tetracarboxylic 3,4:9,10-diimide (PDI-T1)

Perylene-3,4,9,10-tetracarboxylic dianhydride (PTCDA) (1.000 g, 2.56 mmol), **1** (1.701 g, 6.0 mmol), zinc chloride (0.161, 1.18 mmol) and imidazole (3 g, 0.044 mol) were heated under N_2 at 180 °C for 4 h. The reaction mixture was cooled, an aqueous solution of HCl 12 M (20 mL) was added and the reaction system reacted under N_2 for 2 h at 150 °C. The reaction mixture was dispersed in 200 mL of water and basified using an aqueous solution of sodium hydroxide (1 M) to pH 7 at room temperature. The precipitate was collected by filtration and washed with a solution obtained by mixing a 10% (by weight) aqueous solution of HCl (200 mL) with methanol (50 mL). The solid was recovered by filtration and washed by boiling ethanol. The precipitate was collected by filtration and extracted with chloroform by a Soxhlet extraction apparatus. The chloroform solution was concentrated and the product recovered by precipitation in methanol and successive filtration. The product was collected as orange-red powder.

Yield: 40% ^{1}H NMR (400 MHz, $CDCl_3$): (δ ppm) 8.81 (d, J = 8 Hz, 4H), 8.76 (d, J = 8 Hz, 4H), 3.25 (t, J = 3.25 Hz, 4H), 1.95 (m, 4H), 1.43 (m, 40H), 0.93 (t, J = 0.93, 6H). Anal. Calcd. for $C_{54}H_{62}N_6O_4S_2$: C 70.25, H 6.77, N 9.10, S 6.95; found: C 70.12, H 6.63, N 8.73, S 6.80. UV–Vis: (absorption) λ_{max} 460/492/528 nm; (emission) λ_{max} 536/573 nm, Φ_f = 78%.

2.3.4. N,N′-Bis(5-(1-hexyl)nonyl-1,3,4-thiadiazol-2-yl)perylene-3,4,9,10-tetracarboxylic 3,4:9,10-diimide (PDI-T2)

Perylene-3,4,9,10-tetracarboxylic dianhydride (PTCDA) (1.000 g, 2.56 mmol), **2** (1.869, 6.0 mmol), zinc chloride (0.161 g, 1.18 mmol) and imidazole (3 g, 0.044 mol) were heated under N_2 at 180 °C for 4 h. The reaction mixture was cooled, an aqueous solution of HCl 12 M (20 mL) was added and the reaction system reacted under N_2 for 2 h at 150 °C. The reaction mixture was cooled to room temperature, diluted with water and extracted with chloroform. The collected organic layers were extracted with basic NaOH water solution (pH 8). The total collected chloroform layers were dried over Na_2SO_4 and evaporated. The compound was finally purified by column chromatography using silica gel as stationary phase and chloroform/methanol 95/5 as eluent. After solvent evaporation the pure fraction is recovered as an orange-red powder.

Yield: 43% ^{1}H NMR (400 MHz, $CDCl_3$): (δ ppm) 8.75 (m, 8H), 3.35 (m, 2H), 1.85 (m, 8H), 1.45 (m, 40H), 0.92 (m, 12H). Anal. Calcd. for $C_{58}H_{70}N_6O_4S_2$: C 71.13, H 7.20, N 8.58, S 6.55; found: C 70.88, H 7.10, N 8.40, S 6.35. UV–Vis: (absorption) λ_{max} 459/490/526 nm, ε_{max} $4.4 \cdot 10^4$ L mol cm^{-1}; (emission) λ_{max} 535/576 nm, Φ_f = 58%.

2.4. Theoretical calculations

The rotational barrier for the N-(5-methyl-1,2,3-thiadiazole-2-yl) and N-phenyl substituted perylenes was calculated using a constrained optimization: for each fixed value of the dihedral angle ω between the planes of the perylene and of the N-substituent ring, all the molecular internal coordinates were optimized to a minimal electronic energy, within the Born–Oppenheimer approximation. The Density Functional Theory was applied, and the Becke 3 Lin–Yang–Parr [21] hybrid functional was adopted. A split valence double zeta basis set plus polarization functions 6-31G(dp) [22] was used. The calculations were performed using the CRYSTAL 09 suite of computer programs [23].

2.5. Deposition of PDI-T1 and PDI-T2 films

PDI-T1 and PDI-T2 films were evaporated by Knudsen cells in a high-vacuum system ($P = 10^{-7}/10^{-8}$ mbar) on 1 cm^2 substrates with a multilayer structure composed of a thick (500 μm) layer of highly doped Silicon (Si^{2+}) acting both as gate and substrate, a second layer of thermally grown 200 nm thick SiO_2 dielectric layer, interdigitated (source and drain) gold electrodes (bottom-contact configuration) patterned by photolithography processes. The width and the length of the transistor active channels resulted to be equal to 22 mm and 40 μm, respectively. Before the deposition, all Si^{2+}/SiO_2/Au substrates were cleaned by ultrasonic baths in acetone and ethanol, followed by a drying in pure N_2 gas. Some of these substrates were treated by HMDS in order to get hydrophobic surfaces (see Section 2.6). During the film evaporation, the deposition rate was about 1 nm/min (about 0.2 Å/s) and was achieved by keeping the temperature of the bulk material in the cell at 270 °C and the substrate temperature at 90 °C. These conditions were chosen after some trials in such a way to get a reasonable growth rate and prevent any possible thermal decomposition of the molecules. Evaporated films with thickness ranging between 20 and 30 nm were considered in this study. Both deposition rate and thickness were monitored in situ by a quartz crystal microbalance.

Solution processed PDI-T2 films were obtained by spin-coating a hot (~100 °C) solution of PDI-T2 in *o*-dichlorobenzene (10 mg/mL) on HMDS treated Si^{2+}/SiO_2/Au substrates. The solution was spun at 1200 rpm for 1 min. In this way, PDI-T2 films with thickness of about 90 nm were achieved, as checked by AFM microscopy.

2.6. HMDS treatment

To get hydrophobic surfaces, before PDI-T1 and PDI-T2 film deposition, some Si^{2+}/SiO_2/Au substrates were cleaned by immersion in "piranha" solution (a solution obtained

mixing equal volumes of 96% H_2SO_4 and 30% H_2O_2 solutions) at 120 °C for 15 min and then left to cool to room temperature [24]. Subsequently, the substrates were repeatedly rinsed with bi-distilled water, immersed in methanol and sonicated for 10 min. After, the substrates were dipped dichloromethane for 1 min and dried under N_2 flow. Freshly cleaned substrates were put inside a sealed glass vessel, several vacuum-nitrogen cycles were carried out and hexamethyldisilazane (HMDS) (1 mL) was added with a syringe trough a rubber septum. After 4 days, the substrates devices were put off the glass vessel, sonicated both in hexane and methanol for 10 min, dipped in dichloromethane and finally dried under N_2 flow. The self-assembled coupling layer was characterized by advancing aqueous contact angle (θ_a) measurements. The contact angles measured with water were ~110° and are comparable with literature data [25].

2.7. Structural, morphological and electrical characterization

The morphological characterization of the PDI-T1 and PDI-T2 film surfaces was performed by a XE100 Park AFM microscope in air (true non-contact mode with amplitude regulation). Images were acquired using Silicon doped cantilevers (resonance frequency around 300 kHz) provided by Nanosensor™. The root-mean-square (RMS) roughness of the film surface was determined by the Park XEI Software, as the standard deviation of the film height distribution.

X-ray diffraction (XRD) measurements were performed with a Rigaku diffractometer equipped with a conventional CuKα_1 source and a graphite monochromator. The Bragg–Brentano geometry in symmetrical reflection mode was used.

All electrical measurements were performed both in vacuum (10^{-4} mbar) and in air, by using a Janis Cryogenic Probe-Station connected to a Keithley 2612A Dual-Channel system source-meter instrument. During all the electrical measurements, the PDI-T1 and PDI-T2 devices were stored in darkness.

3. Results and discussion

3.1. Synthesis, structural and thermal properties

The new PDI derivatives functionalized at the imide nitrogen with an alkyl-thiadiazole group were synthesized according to the synthetic route shown in Scheme 1. 5-Alkyl-2-aminothiadiazoles were prepared by reaction of the corresponding carboxylic acid with thiosemicarbazide in the presence of $POCl_3$ as the dehydrating agent. Then the system was refluxed with water for 4 h [26]. Afterwards, the PDI derivative was obtained by the condensation reaction of perylene-3,4,9,10-tetracarboxylic dianhydride (PTCDA) with the aminothiadiazole at high temperatures (180 °C) in imidazole as the solvent and in the presence of zinc chloride as a catalyst, under nitrogen atmosphere. After 4 h, a concentrated solution of hydrochloric acid was added and the reaction system further reacted for 2 h at 150 °C.

Functionalization of perylene with the thiadiazole heterocycle was chosen on the basis of two basic issues. First, thiadiazole is a heterocycle known for its electron withdrawing properties [27] that can help in stabilizing, *via* inductive effect, the LUMO energy of the molecule. Indeed, in a recent work [28], a series of soluble PDI derivatives, among which a thiadiazole substituted PDI, were electrochemically investigated: it was found that the thiadiazole substituted PDI has a first reduction potential of about 0.3 V more positive than alkyl derivatives of PDI. This remarkable difference, correlated with a much stable LUMO orbital in thiadiazole containing PDIs, prompted us to investigate whether this kind of material could be a good active layer for ambient working OTFT devices. Cyclic voltammetry experiments were performed on thin films of PDI-T2, the more soluble derivative, in order to confirm this expectation: the redox data were standardized with Ag/AgCl couple. From the onset of the first reduction peak, LUMO energy of −4.30 eV was estimated: this value is consistent with the results described in Ref. [28] and makes PDI-T2 a potential candidate as active layer in ambient stable n-type transistors. HOMO energy of −6.30 eV has been estimated for this molecule by considering the optical bandgap of the film (2.00 eV). Similar conclusions can be drawn for PDI-T1 whose molecular structure differs from that of PDI-T2 only for the length of the alkyl chains. The second issue is related with the pentatomic nature of the thiadiazole heterocycle which, in addition, lacks *ortho*-hydrogen atoms. On these grounds, it is reasonable to assume that the molecular conformation having the heterocycle ring coplanar with the perylene core is accessible in energy and this could lead to a tighter packing that in turn could hinder oxygen penetration and kinetically stabilize the molecule toward oxidation. Substitution at imide nitrogen with a phenyl ring, on the other hand, would induce a twist of the phenyl ring because of close contact of *ortho*-hydrogen atoms with carbonyl oxygen atoms. We have performed theoretical calculations in order to

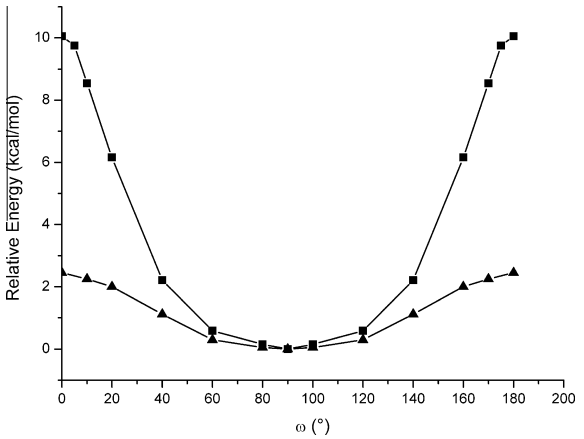

Fig. 1. Relative energy versus dihedral angle for N-substituted perylenes. Line with triangles: N-(5-methyl-1,2,3-thiadiazole-2-yl). Line with squares: N-phenyl. The energies are given in kcal per mol of the N-substituent. The values 0° and 180° of ω correspond to co-planarity of the perylene and N-ring.

check our hypothesis. In Fig. 1, it is reported the energy profile as a function of the lagrangian coordinate ω, identified with the dihedral angle between the plane of the N-aromatic ring and the plane of the perylene core.

In both cases the minimum energy is calculated for the orthogonal orientation of the two planes but, while in the case of the N-phenyl substituted perylene the coplanar or *quasi*-coplanar arrangement is energetically prohibitive ($E > 6$ kcal/mol for $0° < \omega < 20°$) and in fact it has never been found [29], in the case of the N-thiadiazolyl substituted perylene the energy is lower by far: in the same interval of ω it is less than 2.5 kcal/mol and it is within the reach of packing forces.

Thermogravimetric analysis was carried out to investigate the thermal stability of perylene derivatives. The knowledge of the decomposition temperature is fundamental in order to safely perform thermal controlled vacuum evaporation of the derivatives to assemble OTFT device, avoiding conditions that may decompose the active molecules. The measured decomposition temperatures, taken as the temperatures corresponding to 5% weight loss, are quite high: 372 °C and 369 °C for PDI-T1 and PDI-T2, respectively and are about 100 °C higher than the temperature employed for the evaporation procedure (see Section 2).

3.2. Morphological and electrical characterization of OTFT based on PDI-T1 films

Given the poor solubility of the PDI-T1 compound in all common organic solvents, PDI-T1 films were deposited on $Si^{2+}/SiO_2/Au$ substrates for OTFT fabrication only by evaporation. Fig. 2 reports the morphological features of PDI-T1 films evaporated both on bare and HMDS-treated substrates.

Similar to other perylene diimide compounds, evaporated PDI-T1 films exhibit a polycrystalline morphology with the crystalline domains organized in a ribbon-like grain structure. The differences between the films grown on bare and HMDS-treated SiO_2 surfaces are, however, significant. In the former case, the crystallites present basically a regular oval shape with rounded corners and faceted walls. The longest side of any crystalline domain reaches values ranging between 0.8 and 1 μm. The top surface of any island is quite smooth with the presence of extended molecular terraces. In PDI-T1 films grown on

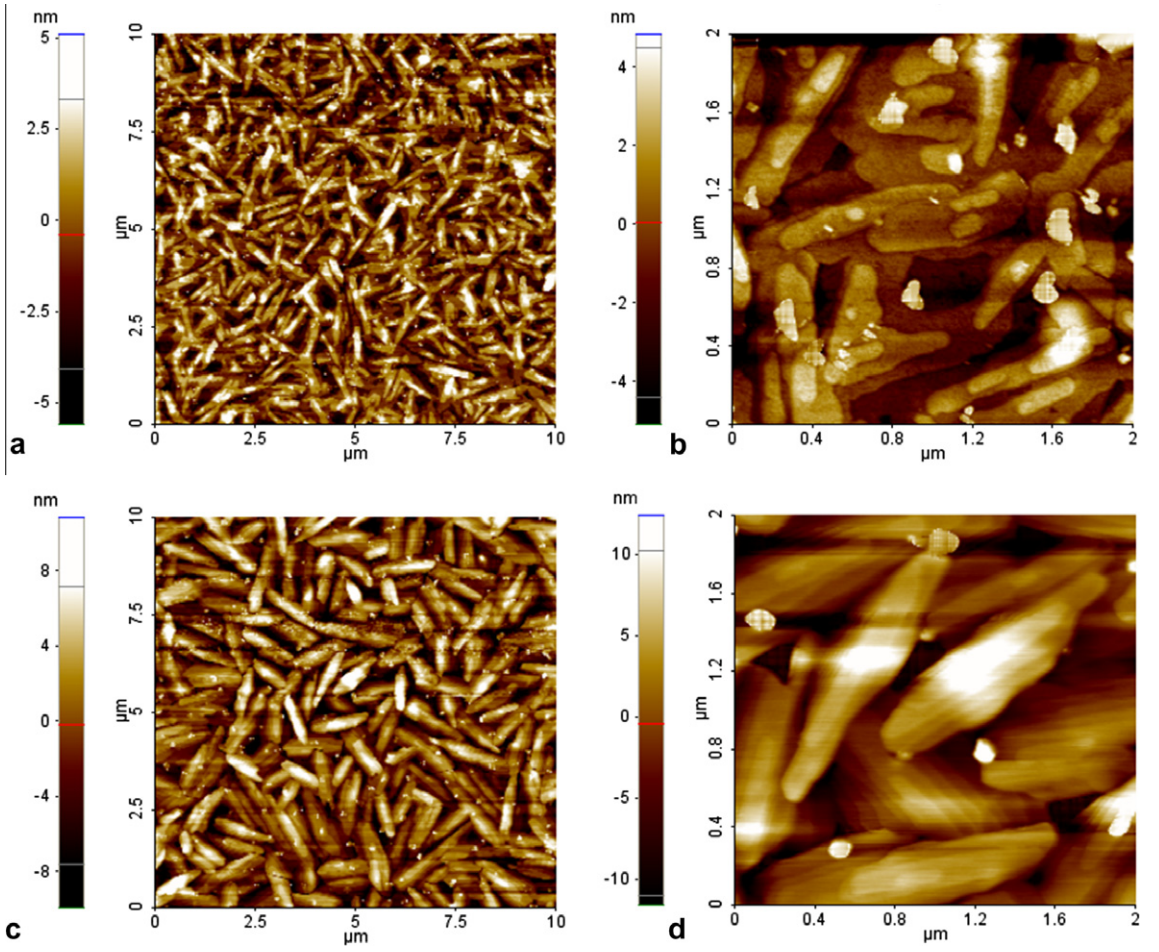

Fig. 2. Atomic Force Microscopy (AFM) images of evaporated PDI-T1 films grown on bare [(a, size 10 μm × 10 μm)-(b, size 2 μm × 2 μm)] and HMDS-treated [(c, size 10 μm × 10 μm)-(d, size 2 μm × 2 μm)] substrates.

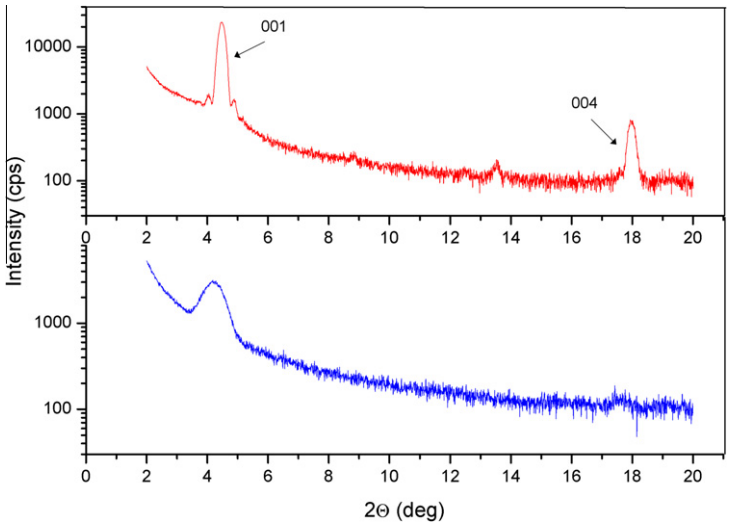

Fig. 3. XRD measurements of evaporated PDI-T1 films on bare (top) and HMDS-treated SiO_2 substrate (bottom).

HMDS-treated substrates, conversely, the crystallites are more elongated in one direction, assuming a peculiar needle-like shape. The crystallite average size increases with the longest side getting maximum values of about 1.5 μm. Moreover, the top surface of any crystalline domain results much less flat. The main features observed in the AFM images are confirmed also in the X-ray spectra recorded for these films using the standard $\vartheta/2\vartheta$ configuration, Fig. 3.

Indeed, multiple reflections from the same Bragg family and Laue oscillations around the (0 0 1) peak are present in the $\vartheta/2\vartheta$ scan for PDI-T1 films grown on HMDS-treated substrates, but they are not observed for films on bare surfaces. This indicates that the crystal structure of PDI-T1 grown on HMDS-treated substrates has higher long-range order and more uniform layer spacing. For films on HMDS-treated SiO_2, the *d*-spacing of lattice planes was also determined from the positions of reflections, giving the value 19.74 Å.

The electrical responses of two PDI-T1 OTFTs fabricated on bare and HMDS-treated substrates are shown in Fig. 4, where both output and transfer-curves measured in vacuum are reported.

The transfer-curves were recorded in the saturation regime by applying V_{DS} = 50 V. These measurements confirm the n-type behavior of the PDI-T1 compound with the charge accumulation taking place for positive V_{GS} voltages. Quite surprisingly, the charge carrier mobility (μ) values, extracted from the transfer-curves by using the standard MOSFET equations [30], were found to be higher for the transistors fabricated on bare substrates. Indeed, the maximum μ values in vacuum were 0.016 and 0.0043 $cm^2/V\,s$ for the devices with bare and HMDS-treated SiO_2, respectively.

This finding can be explained by considering that, despite the PDI-T1 films on HMDS-treated surfaces were composed by larger crystallites, these ordered domains were more spatially isolated and less well connected in comparison to what occurs in the films grown on less hydrophobic surfaces (bare SiO_2). A quantitative confirmation of this feature is given by the values of the surface root-mean-square roughness (R_q) which, for the films on HMDS-treated substrates, was about 3.9 nm, being much higher than the value (R_q = 1.9 nm) estimated for the films grown on bare SiO_2 substrates. Moreover, the typical height of the crystalline domains on HMDS-treated SiO_2 was very close to the nominal film thickness (about 25 nm), giving a clear indication that the boundary regions between the islands were much more extended.

It is worth outlining that the morphological features here evidenced for the PDI-T1 films deposited on HMDS-treated SiO_2 surfaces show some similarities with those of PDI-8CN_2 films deposited on OTS-treated SiO_2 layers, as discussed by Jones et al. [8]. Also in that case, the films grown on the hydrophobic surface, being characterized by needle-like shaped crystalline islands, exhibited a considerably lower mobility value in comparison with that of the transistor on bare SiO_2.

Going back to the electrical features of the PDI-T1 devices, the transistor threshold voltage (V_{TH}) values were estimated according to the MOSFET model by the linear interpolation to zero of the square-root of the transfer-curve measured in the saturation regime (see the inset in Fig. 4b and d). V_{TH} values were slightly negative (typically between 0 and −5 V) for transistors grown on bare SiO_2, while they were positive (typically between 5 and 10 V) for the devices fabricated on HMDS-treated substrates. This behaviour is similar to what found for other perylene diimide derivatives [8] and underscores, also for the PDI-T1 compound, the role of the chemical groups present on the SiO_2 bare surface to induce free charge carriers even in absence of the V_{GS} application. When tested in ambient conditions, all PDI-T1 OTFT fabricated in this work exhibited a clear field effect accumulation, demonstrating their ability to operate even in ambient conditions. However, the analysis of the electrical response in air (performed soon after the device fabrication) revealed that the films grown on bare SiO_2 surface suffered a relevant mobility decrease,

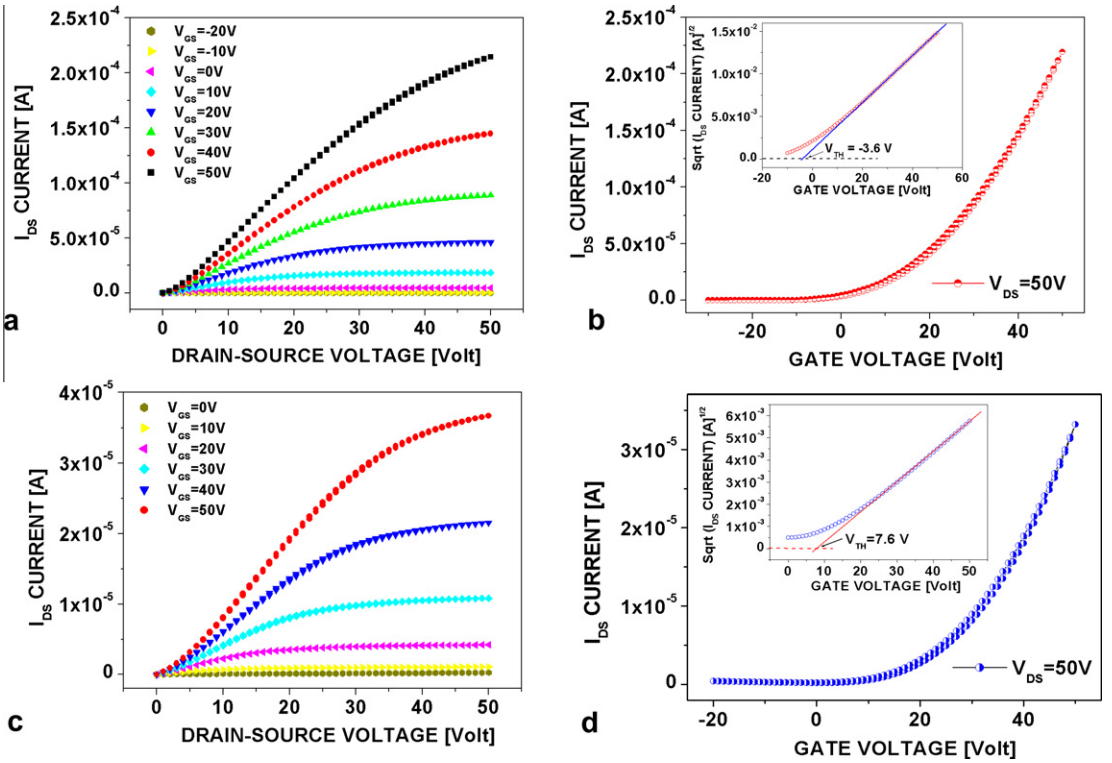

Fig. 4. Output and transfer-curves in saturation measured in vacuum for PDI-T1 transistors fabricated by evaporation on (a, b) bare and (c, d) HMDS-treated substrates.

Table 1
Summary of the electric performances measured in vacuum and air for the PDI-T1 OTFTs.

Transistor	Mobility in vacuum (cm^2/V s)	Mobility in air (cm^2/V s)	On/Off ratio in vacuum	On/Off ratio in air
PDI-T1 (on Bare SiO_2) evaporation	1.6×10^{-2}	2.9×10^{-3}	2.2×10^5	4.6×10^4
PDI-T1 (on HMDS- SiO_2) evaporation	4.3×10^{-3}	3.6×10^{-3}	3.3×10^4	2.6×10^4

with a reduction factor very close to five. On the contrary, for PDI-T1 devices fabricated on HMDS-treated substrates, the mobility degradation in air was much more limited and the difference between the μ values estimated in vacuum and in air did not exceed 20%. Table 1 summarizes the electrical performances of the best PDI-T1 transistors as measured in vacuum and air. This table reports also the on–off current ratios, which have been estimated by considering the maximum and minimum values of the current measured in transfer-curves in the saturation regimes.

3.3. Morphological and electrical characterization of OTFT based on PDI-T2 films

The morphological properties of evaporated PDI-T2 films were found to be very distinctive with large differences in comparison to those observed for PDI-T1 films. As shown in Fig. 5a (see the white circular spots), the morphology of these films is characterized by the presence of columnar structures with height exceeding 30–40 nm (for films with a nominal thickness of 25 nm). In most cases, the section of these nanostructures was almost circular with maximum diameters ranging between 200 and 300 nm.

In the regions external to these nanostructures, the PDI-T2 films displayed apparently a more classical structural organization, given by the coalescence of crystalline islands characterized also by the presence of molecular steps (see, in particular, Fig. 5b). However, the XRD measurements reported in Fig. 6 prompt the idea that the residual degree of crystalline order in these regions is low and developed at very short range. Lattice plane d-spacing for these films was also determined, giving the value 21.2 Å.

No appreciable morphological differences, moreover, were observed by the AFM analysis for PDI-T2 films evaporated on bare or HMDS-treated SiO_2 substrates. In spite of the similar morphology, the electrical performances of the PDI-T2 transistors evaporated on bare and HMDS-treated substrates were quite different (see Fig. 7). In both cases, however, they were much poorer than those achieved with PDI-T1 devices.

The output curves in Fig. 7a and c highlight that the PDI-T2 field-effect transistors were characterized by non-negligible contact resistance effects dominating the behaviour in the low V_{DS} regions, where a diode-like

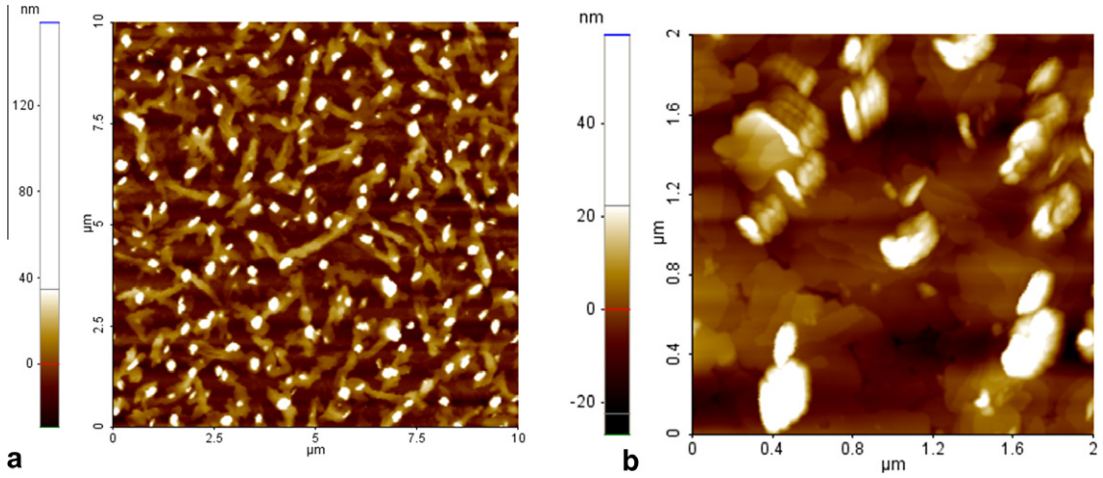

Fig. 5. Atomic Force Microscopy (AFM) images (a, size 10 μm × 10 μm) and (b, size 2 μm × 2 μm) of a PDI-T2 evaporated film on a HMDS-treated substrate.

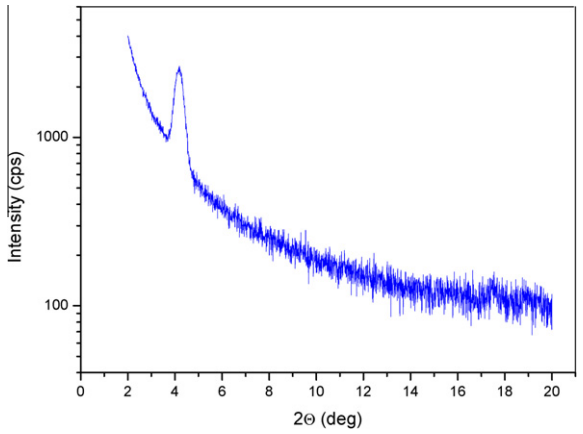

Fig. 6. XRD measurements of a PDI-T2 evaporated film on HMDS-treated SiO_2 substrate.

behaviour, far from the predictions of the ideal MOSFET equations, was observed. In the transfer-curves and in particular for the devices grown on bare substrates, hysteresis phenomena were much more evident than for PDI-T1 transistors.

Maximum mobility values evaluated in vacuum for PDI-T2 films evaporated on bare and HMDS-treated SiO_2 substrates were 1.4×10^{-5} and 7.5×10^{-4} cm^2/V s, respectively. In air, mobility was reduced of about 50% for devices on HMDS-treated substrates, while its degradation was approximately of one order of magnitude for the PDI-T2 OTFTs fabricated on bare SiO_2 surfaces.

The best mobility values as well as the on–off ratios measured in air and vacuum for these transistors are reported in Table 2.

Given these results and the previous morphological analysis revealing the general low crystalline order of the evaporated PDI-T2 films, it comes out that the electrical response of these transistors was mainly ruled by the chemical nature of SiO_2 surface, with the presence of specific groups acting as charge trapping centers. Similar to what found for the PDI-T1 compound (see the inset of Fig. 7b and d), the threshold voltages were negative for PDI-T2 devices on bare substrates and positive in the case of HMDS-treated surfaces. The V_{TH} variation induced by the different hydrophobicity degree of SiO_2 surface was close to 20 V for these evaporated films.

Owing to the solubility of the PDI-T2 compound, field-effect transistors were also fabricated by spin-coating an *o*-dichlorobenzene solution of PDI-T2 on HMDS-treated SiO_2 substrates. The parameters used for the spin-coating deposition are reported in Section 2. Fig. 8 shows the typical morphology of a spin-coated PDI-T2 film. At variance with PDI-T2 evaporated films and similar to what commonly observed for other solution-processed layers, no micro-crystalline structure could be observed in this case. The film surface is characterized only by a very regular corrugation and the average root-mean-square roughness (R_q) was about 10 nm for 90 nm thick films.

The electrical response of a PDI-T2 solution-processed OTFT is reported in Fig. 9.

In this case, the contact resistance effect in the low V_{DS} region seems negligible, likely due to a better coverage of the gold electrodes achieved by the PDI-T2 spin-coated films. Despite this occurrence, the maximum mobility measured in vacuum for these devices was 5.8×10^{-6} cm^2/V s, being about two orders of magnitude lower than the best value found for the evaporated PDI-T2 films. In air, the best mobility value was further reduced down to 3.5×10^{-6} cm^2/V s. The on–off ratio, instead, was similar in air and vacuum being about 80. Finally, these transistors displayed high V_{TH} values, ranging usually between 40 and 50 V.

Both mobility and V_{TH} values measured for the PDI-T2 solution-processed layers suggest that the charge transport in these films was dominated by their low degree of structural order. In this regard, new experimental work devoted to improve the film structural quality by using other solvents and/or following specific annealing procedures is envisaged.

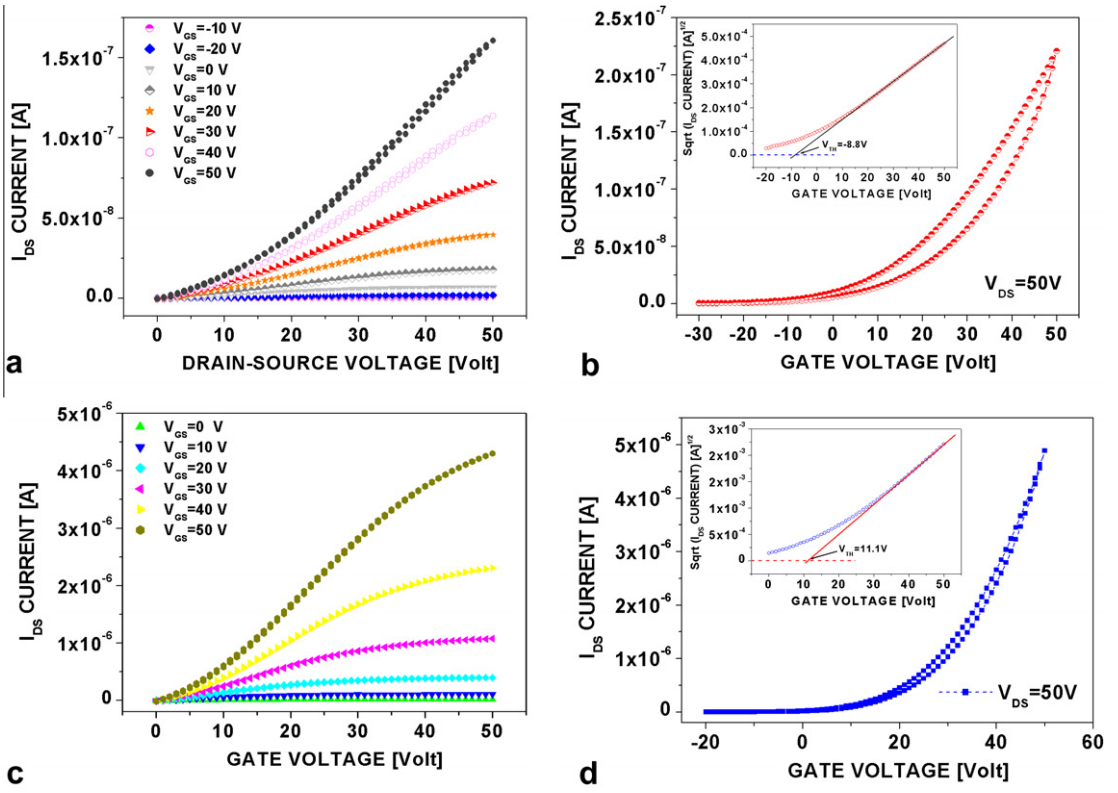

Fig. 7. Output and transfer-curves in saturation measured in vacuum for PDI-T2 transistors fabricated by evaporation on (a, b) bare and (c, d) HMDS-treated substrates.

Table 2
Summary of the electric performances measured in vacuum and air for the evaporated PDI-T2 OTFTs.

Transistor	Mobility in vacuum ($cm^2/V\,s$)	Mobility in air ($cm^2/V\,s$)	On/Off ratio in vacuum	On/Off ratio in air
PDI-T2 (on bare SiO_2) evaporation	1.4×10^{-5}	1.3×10^{-6}	2.2×10^{2}	6.2×10^{1}
PDI-T2 (on HMDS-SiO_2) evaporation	7.5×10^{-4}	3.3×10^{-4}	4.9×10^{3}	1.8×10^{3}

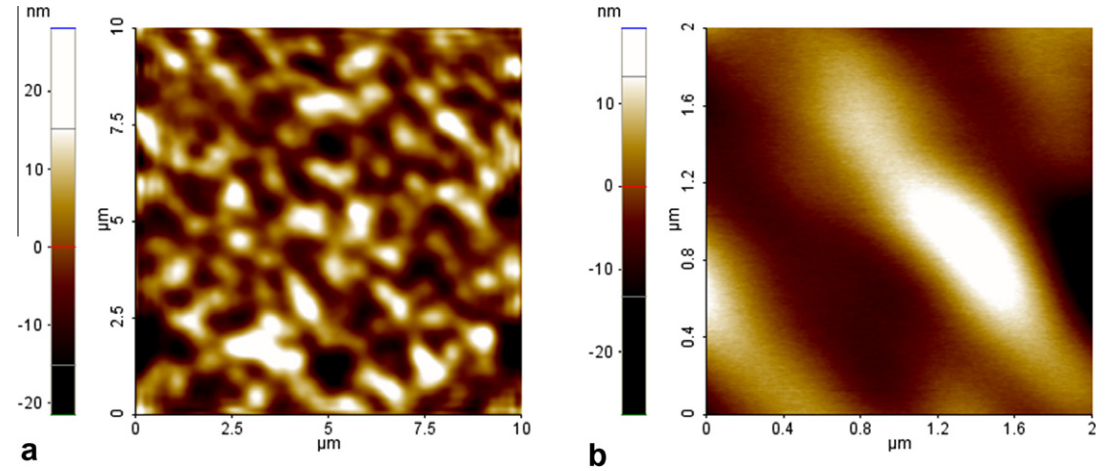

Fig. 8. Atomic Force Microscopy (AFM) images (a, size 10 μm × 10 μm) and (b, size 2 μm × 2 μm) of a PDI-T2 film spin-coated on a HMDS treated substrate.

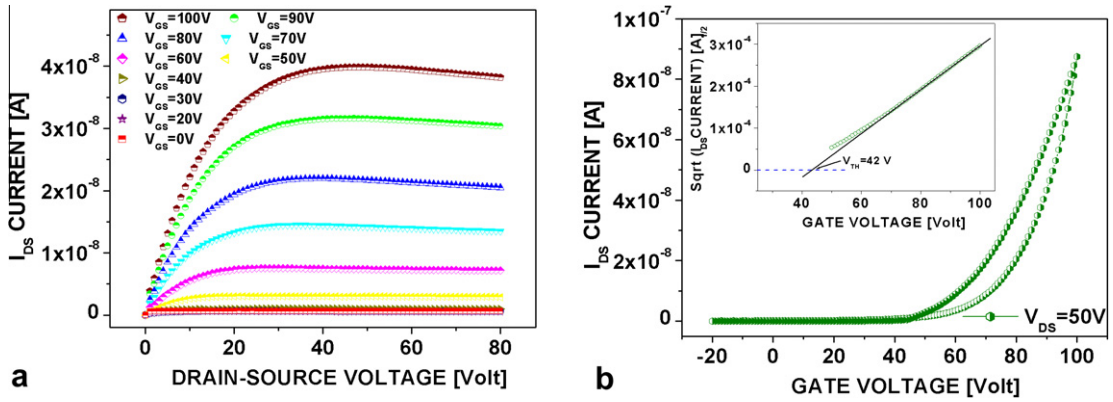

Fig. 9. (a) Output and (b) transfer curves in saturation measured in vacuum for a PDI-T2 transistor fabricated by spin-coating on a HMDS treated substrate.

4. Conclusion

We have demonstrated that both PDI-T1 and PDI-T2 molecules can be used to fabricate n-type transistors able to work even under ambient conditions. PDI-T1 evaporated films exhibited in vacuum a maximum mobility of 0.016 $cm^2/V\,s$ which is comparable with the best values measured for PDI-$8CN_2$ transistors realized by evaporation on the same bottom-contact bottom-gate structure [31]. Similar to other perylene compounds, the electrical characterization of these devices under ambient conditions has shown that an adequate level of hydrophobicity of the dielectric surface is required to preserve the quality of the electrical performances detected in vacuum. Evaporated PDI-T2 films are characterized by a low degree of crystalline order and poorer electrical performances, with mobility values more than one order of magnitude lower than PDI-T1 films. However, by exploiting PDI-T2 solubility in common organic solvents, solution-processed transistors were fabricated. In this case, mobility values between 10^{-6} and $10^{-5}\,cm^2/V\,s$ were estimated.

In conclusion, the possibility to get the charge accumulation effect in air even on bare SiO_2 surfaces, characterized by the high density of electron trapping sites given by specific chemical groups (i.e. hydroxyl SiOH), proves the robustness of the charge transport in these compounds. These experimental findings represent the motivation for future works where the charge transport of other compounds, based on the functionalization of the perylene molecular core with the same thiadiazole rings here considered, will be investigated. In any case, a lot of attention will be paid to optimize the deposition conditions both for the evaporation and the solution techniques with the goal to optimize the electrical performances of OTFT based on these new PDI derivatives.

Acknowledgments

The MIUR of Italy under PRIN 2008 project 2008FSBKKL "Investigation of n-type organic materials and related devices of interest for electronic applications" is gratefully acknowledged for financial support to this research. Thanks are also due to University of Naples "Federico II" and Compagnia San Paolo for financial support under FARO 2010 project.

References

[1] W. Herbst, K. Hunger, Industrial Organic Pigments, third completely revised ed., Wiley WCH, Weinheim, 2004.
[2] E.B. Faulkner, R.J. Schwartz, High Performance Pigments, second revised and expanded ed., Wiley WCH, Weinheim, 2009.
[3] F. Würthner, Chem. Commun. (2004) 1564–1579.
[4] P.R.L. Malenfant, C.D. Dimitrakopoulos, J.D. Gelorme, A. Curioni, W. Andreoni, Appl. Phys. Lett. 80 (2002) 2517–2519.
[5] B.A. Jones, M.J. Ahrens, M.H. Yoon, A. Facchetti, T.J. Marks, M.R. Wasielewski, Angew. Chem. Int. Ed. 43 (2004) 6363–6366.
[6] H.Z. Chen, M.M. Ling, X. Mo, M.M. Shi, M. Wang, Z. Bao, Chem. Mater. 19 (2007) 816–824.
[7] J.H. Ok, S. Liu, Z. Bao, R. Schmidt, F. Wurthner, Appl. Phys. Lett. 91 (2007) 212107.
[8] B.A. Jones, A. Facchetti, M.R. Wasielewski, T.J. Marks, Adv. Funct. Mater. 18 (2008) 1329–1339.
[9] R. Gvishi, R. Reisfeld, Z. Burshstein, Chem. Phys. Lett. 213 (1993) 338–344.
[10] H. Wang, B. Peng, W. Wei, Prog. Chem. 20 (2008) 1751–1760.
[11] W.S. Shi, H.H. Jeong, M.K. Kim, S.H. Jin, M.R. Kim, J.K. Lee, J.W. Lee, Y.S. Gal, J. Mater. Chem. 16 (2006) 384.
[12] H.C. Hesse, J. Weickert, M. Al-Hussein, L. Dössel, X. Feng, K. Müllen, L. Schmidt-Mende, Sol. Energy Mater. Sol. Cells 94 (2010) 560–567.
[13] D.D. Belfield, M.V. Bondar, F.E. Hernandez, F.E. Przhonska, J. Phys. Chem. C 112 (2008) 5618–5622.
[14] M.H. Yoon, S.A. Di Benedetto, M.T. Russell, A. Facchetti, T.J. Marks, Chem. Mater. 19 (2007) 4864.
[15] C. Huang, S. Barlow, S.R. Marder, J. Org. Chem. 76 (2011) 2386–2407.
[16] M. Sadrai, L. Hadel, R.R. Sauers, S. Husain, K. Krogh Jesperson, J.D. Westbrook, G.R. Bird, J. Phys. Chem. 96 (1992) 7988–7996.
[17] (a) F. Würthner, V. Stepanenko, Z. Chen, C.R. Saha-Möller, N. Kocher, D. Stalke, J. Org. Chem. 69 (2004) 7933–7939;
(b) P. Osswald, D. Leusser, D. Stalke, F. Würthner, Angew. Chem. Int. Ed. 44 (2005) 250–253;
(c) R. Schmidt, J.H. Oh, J.-S. Sun, M. Deppisch, A.-M. Krause, K. Radacki, H. Braunschweig, M. Könemann, P. Erk, Z. Bao, F. Würthner, J. Am. Chem. Soc. 131 (2009) 6215–6228.
[18] S. Chai, S.H. Wen, K. Li, Han, Org. Electron. 12 (2011) 1806–1814.
[19] R. Schmidt, M.M. Ling, J.H. Oh, M. Winkler, M. Konemann, Z. Bao, F. Wurthner, Adv. Mater. 19 (2007) 3692–3695.
[20] W.H. Melhuish, J. Phys. Chem. 65 (1961) 229.
[21] A.D. Becke , J. Chem. Phys. 104 (1996) 1040–1046.
[22] M.M. Francl, W.J. Petro, W.J. Hehre, J.S. Binkley, M.S. Gordon, D.J. DeFrees, J.A. Pople, J. Chem. Phys. 77 (1982) 3654.

[23] (a) R. Dovesi, V.R. Saunders, R. Orlando, C.M. Zicovich-Wilson, F. Pascale, B. Civalleri, K. Doll, I.J. Bush, P. D'Arco, M. Lunell, Crystal 2009 User Manual, Turin University, Turin, 2010.;
(b) V.R. Saunders, R. Dovesi, C. Roetti, M. Causa', N.M. Harrison, R. Orlando, C.M. Zicovich-Wilson, Crystal 98 User Manual, Turin University, Turin, 1998.
[24] (a) Q.J. Cai, M.B. Chan-Park, J. Zhang, Y. Gan, C.M. Li, T.P. Chen, B.S. Ong, Org. Electron. 9 (2008) 14–20;
(b) G. Feng, T. Niu, X. You, Z. Wan, Q. Kong, S. Bi, Analyst 136 (2011) 5058–5063.
[25] K. Jeevajothi, D. Crossiya, R. Subasri, Ceram. Int. 38 (2012) 2971–2976.
[26] G. Tu, S. Li, H. Huang, G. Li, F. Xiong, X. Mai, H. Zhu, B. Kuang, W.F. Xu, Bioorg. Med. Chem. 16 (2008) 6663–6668.
[27] H. Pang, P.J. Skabara, D.J. Crown, W. Duffy, M. Heeney, I. McCulluch, S.J. Coles, P.N. Horton, M.B. Hursthouse, Macromolecules 40 (2007) 6585–6593.
[28] G. Türkmen, S. Erten-Ela, S. Icli, Dyes Pigm. 83 (2009) 297–303.
[29] (a) K. Hino, K. Sato, H. Takahashi, S. Suzuki, J. Mizuguchi, Acta Crystallogr. E61 (2005) 0440–0441;
(b) K. Sato, J. Mizuguchi, Acta Crystallogr. E62 (2006) o5008–o5009.
[30] Z. Bao, J. Locklin, Organic Field-Effect Transistors, Taylor & Francis, Boca Raton, 2007.
[31] M. Barra, F.V. Di Girolamo, F. Chiarella, M. Salluzzo, Z. Chen, A. Facchetti, L. Anderson, A. Cassinese, J. Phys. Chem. C 114 (2010) 20387.